

# Prediction of Dynamic and Mixing Characteristics of Drop-Laden Mixing Layers Using DNS and LES

N. Okongo, A. Leboissetier and J. Bellan

Jet Propulsion Laboratory, California Institute of Technology

November 18, 2003

Corresponding Author:

Josette Bellan

Jet Propulsion Laboratory

California Institute of Technology

4800 Oak Grove Drive

M/S 125-109

Pasadena CA 91109-8099 USA

Tel: (818)354-6959, Fax: (818)393-5011

e-mail: [Josette.Bellan@jpl.nasa.gov](mailto:Josette.Bellan@jpl.nasa.gov)

Submitted to 30th International Symposium on Combustion

Colloquium on Heterogeneous Combustion (Sprays)

Short Title: Dynamics and Mixing of drop-laden mixing layers

Paper Length: two-column format

Word Count: Abstract 263; Paper: 5985 (Main Text and Equations 3202 (1455mm); References 319 (145mm); Figures and Captions 2464(1120mm)).

Each Figure with Caption: Fig. 1-117 (53mm) Fig. 2-235 (107mm) Fig. 3-458 (208mm) Fig. 4-503(229mm)  
Fig. 5-458 (208mm) Fig. 6-458(208mm) Fig. 7-235 (107mm).

## Abstract

Direct Numerical Simulation (DNS) and Large Eddy Simulation (LES) have been conducted of a temporal mixing layer laden with evaporating drops, in order to assess the ability of LES to reproduce dynamic and mixing aspects of the DNS which affect combustion, independently of combustion models. The LES uses models for the unresolved Subgrid Scale (SGS) fluxes of species-mass, momentum and heat, and for the filtered source terms (FST) which express the coupling of the drops with the flow. Three SGS-flux models are used: the dynamic-coefficient Smagorinsky (SMD) model, the constant-coefficient Scale-Similarity (SSC) and dynamic-coefficient Gradient (GRD) models. Each LES computational drop represents eight physical DNS drops, and the LES grid spacing is four times that of the DNS. By comparing the filtered and coarsened DNS databases and the LES databases using all SGS models, detailed aspects of the flow that are of interest in ignition or full combustion are analyzed. Global mixture characteristics (the total mass of vapor) are well predicted by all LES models, indicating that these aspects are driven by the resolved, large scale flow. Rotational characteristics (enstrophy and its evolution) and the local thermodynamic state (temperature, equivalence ratio) are not well predicted by the SMD model, which does not capture the small scale physics, but are well predicted by the GRD and SSC models. For all aspects considered, the GRD model predictions are slightly superior to the SSC model, and unlike the SSC model, the GRD model does not require a calibrated coefficient. Thus, the GRD and SSC models show potential for predicting the local flow conditions in combustion problems.

Keywords: large eddy simulation, evaporating drops

# 1 Introduction

Direct Numerical Simulation (DNS), wherein all scales of the flow are resolved, is a methodology for computing turbulent flows without turbulence models, but its utility for three-dimensional turbulent combustion problems is presently limited by the high computational requirements. Large Eddy Simulation (LES), wherein only the large scales need to be resolved, may be a more viable alternative, but has additional modeling requirements to DNS. As a precursor to developing LES models for combustion, LES models first must be developed to accurately predict the mixture thermodynamic state preceding combustion. The temporal mixing layer with evaporating drops provides a flow configuration suitable for developing such LES models, as it embodies transition to turbulence and contains large and small scale variations of thermodynamic quantities, including species composition. Simulating species mixing independently of combustion allows LES errors to be demarcated as resulting from the pre-combustion state rather than from inaccuracies in modeling the combustion process.

For two-phase (TP) flows with drops that are much smaller than the Kolmogorov scale and which have a volumetrically small loading ( $\simeq 10^{-3}$ ), Boivin et al. [1] have shown that the drops can be treated as point sources of mass, momentum and energy from the gas-phase perspective. Then TP simulations can be performed using an Eulerian framework to describe the gas phase and a Lagrangian framework to track the drops, with a gas-phase resolution that is adequate for DNS of single-phase (SP) flow. The terminology ‘DNS’ while not strictly accurate for such TP flows, has been traditionally retained [1]. Several recent studies, e.g. [1–7], have used this DNS methodology.

For evaporating drops, phase change leads to thermodynamic variations that necessitate a compressible formulation. Because the density of the drop liquid is large compared to that of the carrier gas, the mass loading may be significant ( $\gtrsim 10^{-1}$ ) and thus the drops may considerably influence the flow (two-way coupling). DNS for these conditions has recently been performed to develop LES models [7]. The LES gas-phase equations are derived by filtering the DNS gas-phase equations, leading to unclosed terms: the SGS fluxes that arise from the convective terms and the filtered source terms (FSTs) that contain the drop effect on the gas phase. Using DNS-derived models, LES has then been conducted with reduced flow field resolution compared to DNS and using ‘computational’ drops to represent the DNS physical drops [8]. In this

paper, we compare the dynamic and mixing characteristics from the DNS database [7] to the LES results [8] to assess the LES rendering of features that are important for combustion. Following the summary of the LES method in Section 2, details of the comparison are described in Section 3, with conclusions in Section 4.

## 2 LES Method

Details of the DNS and LES methods have been given by Okong'o and Bellan [7], based on the DNS formulation of Miller and Bellan [4]. The LES uses the same mathematical description as the DNS, i.e. Eulerian for the gas phase and Lagrangian for the liquid phase. The LES gas-phase conservative variables are obtained by spatially filtering the DNS field using a top-hat filter; this filtering is denoted by an overbar. The LES field variables are  $\bar{\phi} = \{\bar{\rho}, \bar{\rho}\tilde{u}_i, \bar{\rho}\tilde{e}_t, \bar{\rho}\tilde{Y}_V\}$  where  $\rho$  is the density,  $u_i$  is the velocity in the  $x_i$  coordinate direction,  $e_t$  is the total energy and  $Y_V$  is the vapor mass fraction (the carrier gas mass fraction is  $Y_C$ ;  $Y_C + Y_V = 1$ ), and the tilde denotes Favre (density-weighted) filtering (e.g.  $\tilde{u}_i = \overline{\rho u_i} / \bar{\rho}$ ). The pressure ( $p$ ), temperature ( $T$ ) and enthalpy ( $h = e + p/\rho$ ) are computed from the internal energy ( $e = e_t - u_i u_i / 2$ ), assuming calorically perfect gases. The viscosity  $\mu$ , the diffusion coefficient  $D$  and the thermal conductivity  $\lambda$  are assumed constant, and are defined through the Prandtl and Schmidt numbers. The LES computational drop field is  $\bar{Z} = \{X_i, v_i, T_d, m_d\}$ , with position  $X_i$ , velocity  $v_i$ , temperature  $T_d$ , and mass  $m_d$  for each drop.

### 2.1 Liquid phase

The LES uses  $N_{cd}$  computational drops to represent the  $N_d$  physical drops, that is each computational drop represents  $N_R \equiv N_d / N_{cd}$  physical drops. The LES computational drops, tracked in a Lagrangian frame, follow the same evolution equations governing the physical drops (see [4]):

$$d\bar{Z}/dt = \Sigma(\tilde{\psi}_f, \tilde{\psi}_s, \bar{Z}), \quad (1)$$

$$\Sigma = \left\{ v_i, \frac{F_i}{m_d}, \frac{Q + \dot{m}_d L_V}{m_d C_L}, \dot{m}_d \right\}. \quad (2)$$

$\Sigma$  has the same functional form as in the DNS but is based on  $\tilde{\psi}$  instead of  $\psi$ ;  $F_i$  is the drag force,  $Q$  is the heat flux,  $\dot{m}_d$  is the evaporation rate, and  $C_L$  is the heat capacity of the liquid.  $L_V$  is the latent heat of vaporization, here a linear function of temperature,  $L_V = h_V^0 - (C_L - C_{p,V})T_d$ ,  $h_V^0$  is the reference

vapor enthalpy which accounts for the enthalpy difference between the vapor and carrier gas and  $C_{p,v}$  is the vapor constant-pressure heat capacity. The drop evolution depends on the gas-phase primitive variables,  $\psi(\phi) = \{u_i, T, Y_V, p\}$ , evaluated either at the drop surface (subscript  $s$ ) or at the drop far-field (subscript  $f$ ). The far-field variables are taken as the gas-phase primitive variables interpolated to the drop locations. The detailed expressions for  $F_i$ ,  $Q$ , and  $\dot{m}_d$  involve validated Stokes-drag-based correlations for point drops [4], with the particle time constant defined as  $\tau_d = \rho_L d^2 / (18\mu)$  [9], where  $\rho_L$  is the liquid density and  $d$  is the drop diameter ( $m_d = \rho_L \pi d^3 / 6$ ). The Stokes drag is empirically corrected for finite drop Reynolds numbers, while the Nusselt and Sherwood numbers are empirically modified for convective corrections to heat and mass transfer based on the Ranz-Marshall correlations [4].

## 2.2 Gas phase

The LES gas-phase equations are:

$$\begin{aligned} & \partial \bar{\phi} / \partial t + \partial (\bar{\phi} \tilde{u}_j) / \partial x_j \\ & = \partial [\theta_j(\bar{\phi}) + \theta_{SGS,j}] / \partial x_j + \bar{S}, \end{aligned} \quad (3)$$

where  $\bar{S} = \{\bar{S}_I, \bar{S}_{II,i}, \bar{S}_{III}, \bar{S}_I\}$ ,

$$\begin{aligned} \theta_j(\phi) &= \{0, -p\delta_{ij} + \sigma_{ij}, \\ & \quad (-pu_j - q_j + \sigma_{ij}u_i), -j_V\}; \\ \theta_{SGS,j} &= \{0, -\bar{\rho}\tau_{ij}, \\ & \quad (-\bar{\rho}\zeta_j - \bar{\rho}\tau_{ij}\tilde{u}_i), -\bar{\rho}\eta_j\}; \\ \tau_{ij} &= \widetilde{u_i u_j} - \tilde{u}_i \tilde{u}_j, \quad \zeta_j = \widetilde{h u_j} - \tilde{h} \tilde{u}_j, \\ \eta_j &= \widetilde{Y_V u_j} - \tilde{Y}_V \tilde{u}_j, \end{aligned}$$

$\sigma$  is the viscous stress,  $\mathbf{q}$  is the heat flux, and  $j_V$  is the vapor mass flux. In Eq. 3, the FSTs ( $\bar{S}$ ) and the SGS fluxes ( $\tau_{ij}$ ,  $\zeta_j$ ,  $\eta_j$ ) must be modeled. The adopted FST model, for a top-hat filter, is [7]

$$\bar{S} = N_R \sum_{\beta=1}^{N_\beta} (1/V_f) [S_d(\tilde{\psi}(\bar{\phi}), \bar{Z})]_\beta, \quad (4)$$

where the summation is over the  $N_\beta$  computational drops within the filtering volume  $V_f$ .  $S_d = \{S_{I,d}, S_{II,i,d}, S_{III,d}, S_{I,d}\}$  has the same functional form as in the DNS but, being based on  $\tilde{\psi}$  instead of  $\psi$ , does not contain SGS effects:

$$\begin{aligned} S_{I,d} &= -\dot{m}_d, & S_{II,i,d} &= -F_i - \dot{m}_d v_i, \\ S_{III,d} &= -F_i v_i - Q - \dot{m}_d (v_i v_i / 2 + h_{V,s}) \end{aligned}$$

where  $h_{V,s}$  is the vapor enthalpy at the drop surface. Three SGS-flux models are considered: dynamic Gradient (GRD), dynamic Smagorinsky (SMD), and constant coefficient scale-similarity (SSC) [10–12].

### 2.3 Configuration and procedure

The mixing layer geometric configuration is illustrated in Fig. 1, where the streamwise ( $x_1$ ), the cross-stream ( $x_2$ ), and the spanwise ( $x_3$ ) coordinates are shown. Periodic boundary conditions are used in the  $x_1$  and  $x_3$  directions, and adiabatic slip wall conditions are employed for the  $x_2$  boundaries. To promote layer growth, the layer is initially perturbed so as to induce roll-up and pairing. The evolution of the layer comprises two pairings for the four initial spanwise vortices to form a single vortex. Initially, the gas phase consists only of the carrier gas (air;  $\rho_0=0.9415\text{kg/m}^3$ ). The drops (n-decane;  $\rho_L=642\text{kg/m}^3$ ) are initially distributed randomly throughout the  $x_2 < 0$  domain; each drop initially has the same velocity as the gas phase at its location. The initial vorticity thickness is  $\delta_{\omega,0} = \delta_\omega(0)$  where  $\delta_\omega(t) = \Delta U_0 / (\partial \langle u_1 \rangle / \partial x_2)_{\max}$ , with  $\langle \rangle$  denoting averaging over homogeneous ( $x_1, x_3$ ) planes and  $\Delta U_0 = 2U_0$  being the velocity difference across the layer; the initial mean streamwise velocity has an error-function profile.

From the DNS database [7], two DNS cases with  $\text{Re}_0 = \rho_0 \Delta U_0 \delta_{\omega,0} / \mu = 600$  but differing initial mass loadings  $ML_0$  are considered: TP600a2 ( $N_d = 2993630$ ,  $N_{cd} = 374203$ ,  $ML_0 = 0.2$ ) and TP600a5 ( $N_d = 7484075$ ,  $N_{cd} = 935509$ ,  $ML_0 = 0.5$ ). All cases have convective Mach number of 0.35,  $\delta_{\omega,0} = 6.859 \times 10^{-3}\text{m}$  and domain size of  $0.2\text{m} \times 0.22\text{m} \times 0.12\text{m}$ . DNS use  $288 \times 320 \times 176$  points; LES use  $72 \times 80 \times 44$  points ( $\Delta x_{LES} = 4\Delta x_{DNS}$ ), the filter width  $\bar{\Delta} = 2\Delta x_{LES}$  and  $N_R = 8$ . Initially, all the drops are at 345K, being colder than the initial carrier gas temperature (375K) and the liquid boiling temperature (447.7K) to promote evaporation. The drop size is specified through the drop Stokes number  $St = \tau_d \Delta U_0 / \delta_{\omega,0}$ , which initially has Gaussian distribution with mean 3 and standard deviation 0.5.

The LES are performed using the same numerical scheme as the DNS: fourth-order explicit Runge-Kutta temporal integration for time derivatives, eighth-order central finite differences with tenth-order filtering for spatial derivatives [13], and fourth-order Lagrange interpolation to obtain gas-phase variable values at the drop locations. The LES results are compared to the filtered coarsened (FC) DNS having the same grid points, which also provides the LES initial condition. In the SMD and GRD models, the model coefficient is computed from the LES solution using refiltering at test-filter width  $\hat{\Delta} = 2\bar{\Delta}$ ; the SSC model uses  $\hat{\Delta} = \bar{\Delta}$  and the DNS-calibrated coefficient  $C_{SS} = 1.996$  [7]. Most of the analysis is performed at the DNS transitional time,  $t_{trans}^* = 105$ , at which time the DNS momentum-thickness Reynolds number is approximately 1570. Given the considerably lower CPU requirements for LES compared to DNS (up to a factor of 120 shorter CPU time), the interest is whether flow features pertinent to combustion are accurately predicted by LES.

### 3 Results

#### 3.1 Dynamic Characteristics

To assess the dynamic characteristics of the layers, plotted in Fig. 2 is the evolution of the resolved enstrophy ( $\omega \cdot \omega$ ), averaged over the domain, for TP600a2 and TP600a5. For convenience, the tilde and overbar denoting filtered quantities are omitted; it is to be understood that all quantities discussed below are either filtered quantities or computed from filtered quantities. Both  $ML_0$  layers have similar  $\langle\langle\omega \cdot \omega\rangle\rangle$  evolution, although the peak is slightly higher for TP600a5. Comparing the LES results, the SMD model clearly has minimal enstrophy generation, while the GRD and SSC models have significantly more. Both GRD and SSC LES qualitatively match the FC-DNS in having an initial increase after rollup, followed by decline after the second pairing. However the SSC peaks sooner and at a lower value and decays faster, compared to the GRD which better matches the FC-DNS. Plots of  $\omega \cdot \omega$  in the between-the-braid plane at the DNS transition time, Fig. 3, show the GRD to also have more of the small scale features observed for the FC-DNS. In contrast to the FC-DNS, the SMD shows little small scale activity, only large scale structures resulting from pairing.

The  $(\boldsymbol{\omega} \cdot \boldsymbol{\omega})$  budget

$$\begin{aligned}
& D(\boldsymbol{\omega} \cdot \boldsymbol{\omega})/Dt \\
= & 2\boldsymbol{\omega} \cdot [(\boldsymbol{\omega} \cdot \nabla) \mathbf{u}] - 2(\boldsymbol{\omega} \cdot \boldsymbol{\omega})(\nabla \cdot \mathbf{u}) \\
& + 2\boldsymbol{\omega} \cdot [\nabla \times (-\nabla p - \nabla \cdot \boldsymbol{\sigma})/\rho] \\
& + 2\boldsymbol{\omega} \cdot [\nabla \times (\mathbf{S}_{II,i} - \mathbf{u}S_I)/\rho]
\end{aligned} \tag{5}$$

contains six terms—stretching/tilting, dilatation, baroclinic, viscous, mass source, and momentum source terms. Homogeneous-plane averages of these terms, computed on the FC-DNS and LES fields and plotted in Fig. 4, show the GRD model to best reproduce the FC-DNS. Again, the SSC results are qualitatively similar to the GRD, but with smaller magnitude and cross-stream extent. As for the FC-DNS, these LES predict that the largest contribution to  $(\boldsymbol{\omega} \cdot \boldsymbol{\omega})$  arises from the stretching and tilting, on average positive, counteracted by the mostly negative and smaller viscous effect. While at first glance the SMD shows reasonable agreement with the other two models, further examination reveals that its curves are smoother, due to the lack of small scale variations, and there is a dip in the stretching/tilting term near the upper stream. Additionally, compared to the GRD and SSC, the SMD has larger magnitude of source term contributions and a smaller magnitude viscous term relative to the stretching/tilting term.

The spatial extent of vorticity activity in the domain, which is due to the largest scale vortical structures, is captured by all models. However, unlike the GRD and SSC models, the SMD model does not capture the small-scale vorticity structure.

### 3.2 Mixing Characteristics

Of interest in combustion applications is the local thermodynamic state, in particular the temperature and equivalence ratio determining the propensity for reaction. The equivalence ratio is defined as  $\Phi = (M_F/M_O)/(M_F/M_O)_{st}$ , where  $M_F$  and  $M_O$  denote the mass of the fuel and oxidizer respectively, and  $st$  indicates the stoichiometric conditions; locally,  $\Phi = (Y_V/Y_C)/(Y_V/Y_C)_{st}$ . For the air-decane reaction,  $\text{C}_{10}\text{H}_{22} + 15.5(\text{O}_2 + 3.76\text{N}_2) \rightarrow 10\text{CO}_2 + 11\text{H}_2\text{O} + 58.28\text{N}_2$ ,  $(Y_V/Y_C)_{st} = 0.316$ . Considering the temperature contours, Fig. 5, the SMD LES has a wider range of temperatures compared to the FC-DNS, while the GRD

and SSC are too cold in the lower stream. As in the enstrophy, the SMD temperature lacks small scale activity, and the observed variations are due to the large scale mixing. A similar plot of the equivalence ratio, in Fig. 6, likewise shows little small scale activity for SMD and an overprediction of  $\Phi$ . The GRD and SSC also overpredict  $\Phi$ , but not as much.

Finally, the global equivalence ratio  $\Phi = (M_V/M_C) / (M_V/M_C)_{st}$  is plotted in Fig. 7, where  $M_V$  and  $M_C$  are the total mass of vapor and carrier gas, respectively, in the domain. All three LES have excellent global predictions that closely follow the FC-DNS, although the GRD and SSC models tend to slight overprediction. In view of the contour plots, these global results need to be interpreted with caution; clearly the global mixture state is much better predicted than the details. The global state is due mainly to the largest-scale mixing, which is independent of the SGS model, while an accurate SGS model is crucial to replicate the local state, which is of prime importance for combustion simulations.

## 4 Conclusions

DNS and LES results have been compared for a temporal mixing layer laden with evaporating drops to elucidate dynamic and thermodynamic features crucial to combustion. The LES used dynamic Smagorinsky (SMD), dynamic Gradient (GRD) or constant-coefficient Scale-Similarity (SSC) models for the SGS fluxes in the LES gas-phase equations. The SSC coefficient was calibrated on the DNS database, while the SMD and GRD model coefficients were computed from the LES field during the LES. The LES used computational drops, whose effect on the flow field occurred through filtered source terms in the LES gas-phase equations; each LES drop represented eight physical drops. The LES grid spacing was four times that of the DNS. An examination of the dynamic and mixing characteristics showed that all LES predict well the global ratio of fuel-to-vapor mass, indicating the proper amount of global drop evaporation. In this mixing layer configuration, the largest scale vortices are primarily responsible for drop entrainment and control the large scale mixing, and thus some global aspects will be captured regardless of the LES model. However, the SMD model was shown incapable of portraying the correct small-scale physics, both in the dynamic characteristics (enstrophy and enstrophy generation) and in the local thermodynamic state (temperature and equivalence ratio). The GRD and SSC models did capture these characteristics, with the GRD model being somewhat

superior. Therefore, the GRD and SSC models are expected to perform better in combustion problems, which are driven by the local flow field state.

## Acknowledgements

This work was conducted at the Jet Propulsion Laboratory (JPL) of the California Institute of Technology under the sponsorship of the U.S. Department of Energy (contract monitors R. Danz and D. Hooker), under an agreement with the National Aeronautics and Space Administration. Computations were performed on the JPL Supercomputing Center SGI Origin 2000.

## References

- [1] M. Boivin, O. Simonin, and K. Squires, *J. Fluid Mech.*, 375(1998) 235–263.
- [2] F. Mashayek, *J. Fluid Mech.*, 367 (1998) 163–203.
- [3] F. Mashayek, F.A. Jaber, *I. J. Heat Mass Transfer*, 42 (1999) 2823–2836.
- [4] R. Miller, J. Bellan, *J. Fluid Mech.*, 384 (1999) 293–338.
- [5] R. Miller, J. Bellan, *Phys. Fluids*, 12(3) (2000) 650–671.
- [6] J. Réveillon, L. Vervisch, *Combust. Flame*, 121 (2000) 75–90.
- [7] N. Okong'o, J. Bellan. Consistent large eddy simulation of a temporal mixing layer laden with evaporating drops. Part 1: Direct numerical simulation, formulation and *a priori* analysis. *J. Fluid Mech.* (2003) to appear.
- [8] A. Leboissetier, N. Okong'o, J. Bellan. Consistent large eddy simulation of a temporal mixing layer laden with evaporating drops. Part 2: *A Posteriori* analysis. (2003) to be submitted.
- [9] C. Crowe, J. Chung, T. Troutt, *Prog. Energy Combust. Sci.*, 14 (1998) 171–194.
- [10] R. Clark, J. Ferziger, W. Reynolds, *J. Fluid Mech.*, 91(1) (1979) 1–16.

- [11] J. Smagorinsky. In B. Galperin, S. Orszag, (Eds.), *Large Eddy Simulation of Complex Engineering and Geophysical Flows*. Cambridge University Press, 1993, pp. 3–36.
- [12] J. Bardina, J. Ferziger, W. Reynolds, Improved subgrid scale models for large eddy simulation, AIAA 80-1357 (1980).
- [13] C. Kennedy, M. Carpenter, *Appl. Num. Maths*, 14 (1994) 397–433.

## LIST OF FIGURE CAPTIONS

1. Mixing Layer Configuration
2. Evolution of global enstrophy: FC-DNS (■), GRD (---), SMD (-.-), SSC (-...-)
3. Enstrophy  $(\omega \cdot \omega) (\delta_{\omega,0}/\Delta U_0)^2$ : Between-the-braid plane TP600a5,  $t^*=105$ .
4. Enstrophy budget, non-dimensionalized by  $(\delta_{\omega,0}/\Delta U_0)^3$ : plane average TP600a5,  $t^*=105$ .  $2\omega \cdot [(\omega \cdot \nabla) \mathbf{u}]$   
 (—);  $-2(\omega \cdot \omega)(\nabla \cdot \mathbf{u})$  (-.-);  $-2\omega \cdot [\nabla \times (\nabla p/\rho)]$  (-...-);  $2\omega \cdot \{\nabla \times [(\nabla \cdot \sigma)/\rho]\}$  (···);  $2\omega \cdot [\nabla \times (\mathbf{S}_{II,i}/\rho)]$   
 (— —);  $-2\omega \cdot [\nabla \times (\mathbf{u}S_I/\rho)]$  (- - -)
5. Temperature: Between-the-braid plane TP600a5  $t^*=105$ .
6. Equivalence Ratio,  $\Phi$ : Between-the-braid plane TP600a5,  $t^*=105$ .
7. Evolution of global equivalence ratio: FC-DNS (■), GRD (---), SMD (-.-), SSC (-...-)

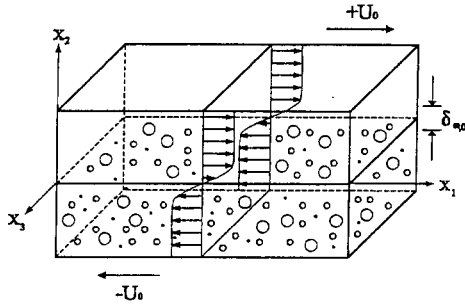


Figure 1: Mixing Layer Configuration

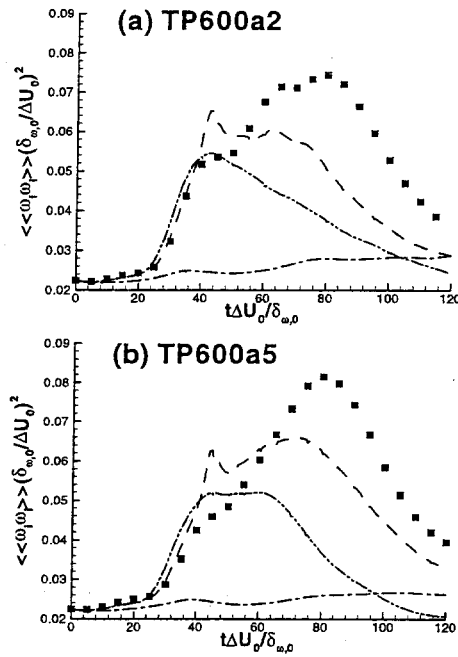


Figure 2: Evolution of global enstrophy: FC-DNS (■), GRD (---), SMD (-.-), SSC (-.-.-)

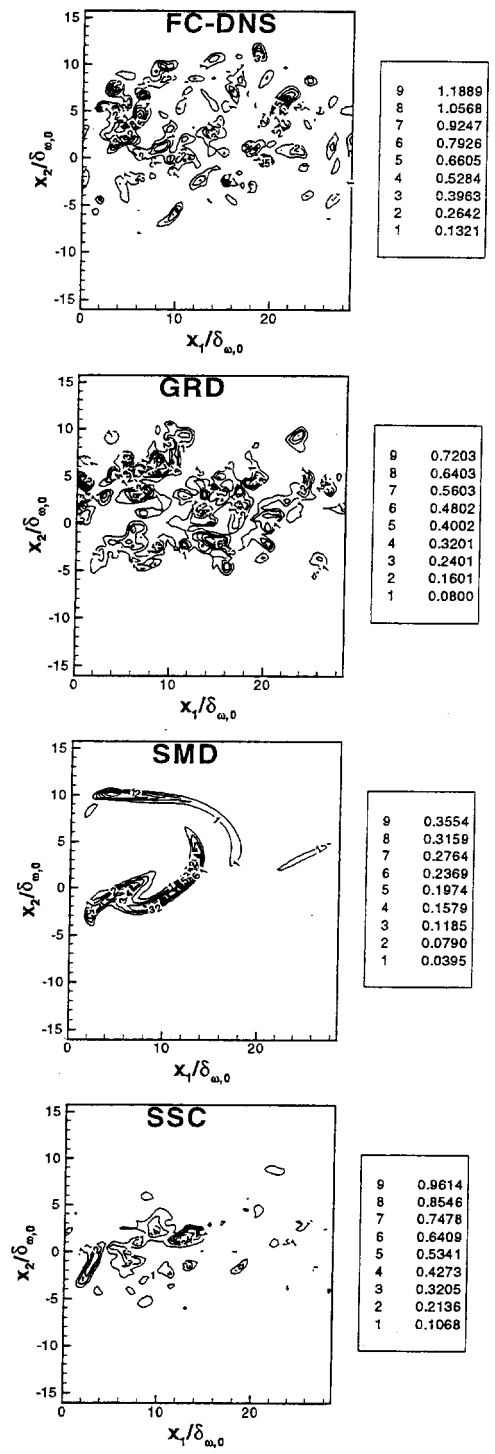


Figure 3: Enstrophy  $(\omega \cdot \omega) (\delta_{\omega,0}/\Delta U_0)^2$ : Between-the-braid plane TP600a5,  $t^*=105$ .

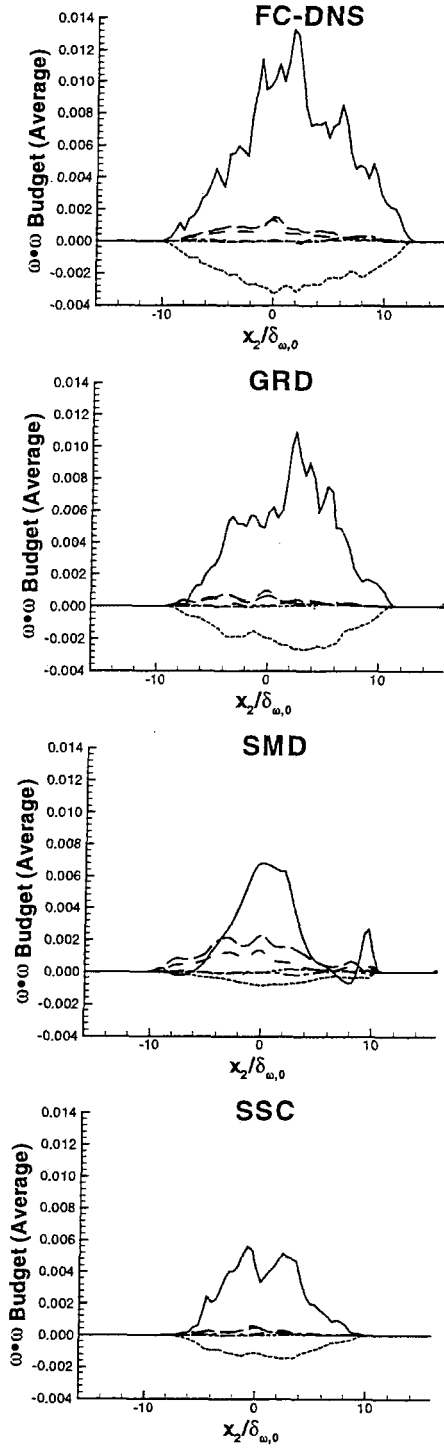
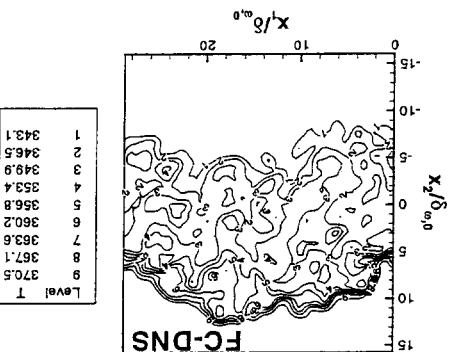
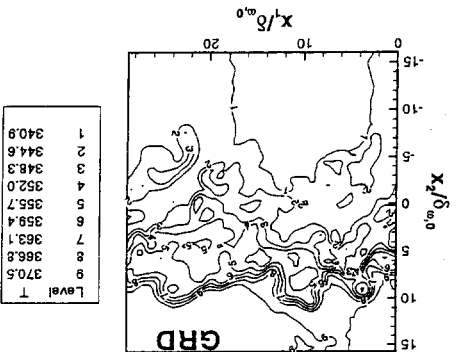
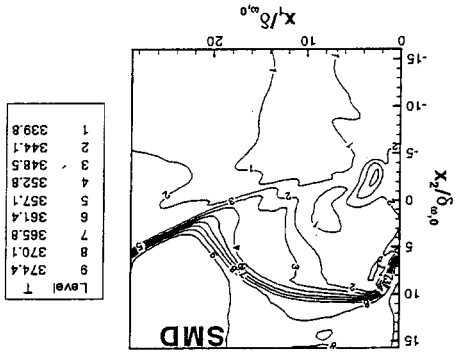
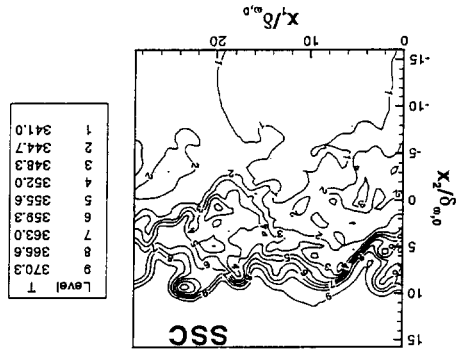


Figure 4: Enstrophy budget, non-dimensionalized by  $(\delta_{\omega,0}/\Delta U_0)^3$ : plane average TP600a5,  $t^*=105$ .

$2\omega \cdot [(\omega \cdot \nabla) \mathbf{u}]$  (—);  $-2(\omega \cdot \omega)(\nabla \cdot \mathbf{u})$  (- - -);  $-2\omega \cdot [\nabla \times (\nabla p/\rho)]$  (- · · -);  $2\omega \cdot \{\nabla \times [(\nabla \cdot \sigma)/\rho]\}$  (···);

$2\omega \cdot [\nabla \times (\mathbf{S}_{II,i}/\rho)]$  (— —);  $-2\omega \cdot [\nabla \times (\mathbf{u}S_I/\rho)]$  (- - -)

Figure 5: Temperature: Between-the-braid plane TP600a5  $\tau=105$ .



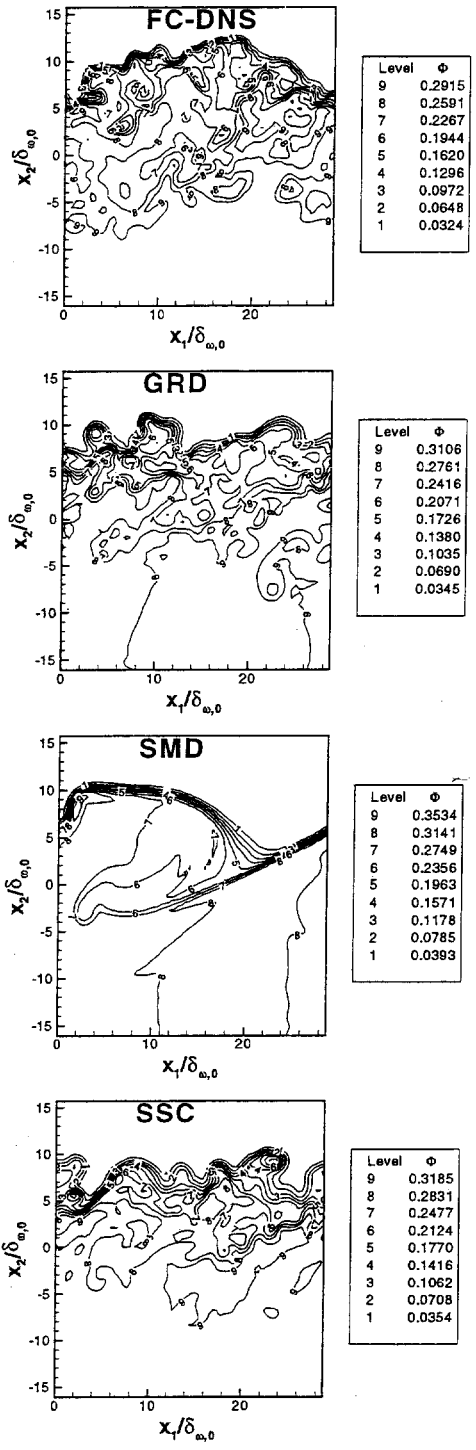


Figure 6: Equivalence Ratio,  $\Phi$ : Between-the-braid plane TP600a5,  $t^*=105$ .

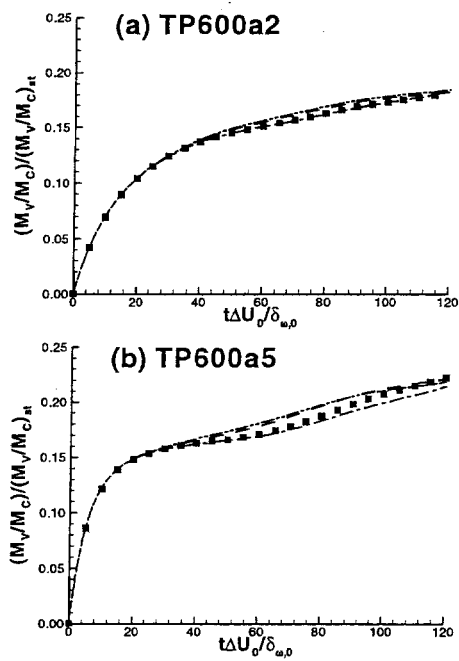


Figure 7: Evolution of global equivalence ratio: FC-DNS (■), GRD (---), SMD (-.-), SSC (-.-.-)